Chemical Science

RSCPublishing

ARTICLE

Pd-η^3-C_6H_9 Complexes of the Trost Modular Ligand: High Nuclearity Columnar Aggregation Controlled by Concentration, Solvent and Counterion.

Cite this: DOI: 10.1039/x0xx00000x

Received 00th January 2012,
Accepted 00th January 2012

DOI: 10.1039/x0xx00000x

www.rsc.org/

Daugirdas Tomas Racys,[a] Julian Eastoe,[b] Per-Ola Norrby[c] and Guy C. Lloyd-Jones.*[d]

The Trost modular ligand (TML) series induces high levels of asymmetric induction in an extraordinarily wide range of reactions involving palladium π-allyl intermediates. Prior mechanistic investigations into reactions involving simple Pd-π-cyclohexenyl intermediates has focussed on the monomeric 13-membered ring formed via P,P-chelation of the ligand to Pd. However, ring-opening oligomerisation was recognised as providing a major pool of polynuclear palladium species that, through low or even opposite asymmetric induction to the mononuclear species, are responsible for a reduction in selectivity under non-optimised conditions. Herein we describe an investigation by NMR, molecular mechanics, molecular dynamics, and small-angle neutron scattering, of a Pd-π-cyclohexenyl cation bearing the 1,2-diaminocyclohexane TML ligand (**2**). Using both nondeuterated and perdeuterated (D_{47}) isotopologues of the resulting complexes ($[\mathbf{1}]^+$), we show that a two-stage oligomerisation-aggregation process forms large cylindrical particles of high nuclearity (up to 56 Pd centres).

Introduction

The Trost modular ligand (TML) series[1] has been applied to an extraordinarily wide range of Tsuji-Trost (allylic alkylation) reactions.[2] Under carefully optimised conditions, these ligands frequently provide high enantioselectivity in reactions that have proven challenging with other chiral ligands, particularly those involving cyclic allylic substrates.[3-6] These features have led to broad use of the TML in the synthesis of natural products,[7] as well as industrial application for the construction of high enantiopurity chiral building blocks. However, reactions involving the TML frequently exhibit, memory effects[8,9] and a high sensitivity of the enantioselectivity to reaction temperature, catalyst concentration, solvent and nucleophile counter-ion.

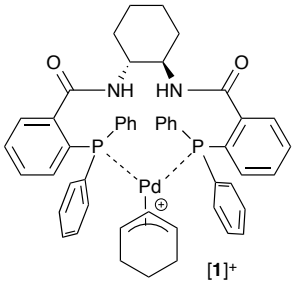

$[\mathbf{1}]^+$

Our previous mechanistic studies of this system focussed on the *monomeric* cationic complex $[\mathbf{1}]^+$, in which the 1,2-diaminocyclohexane derived TML ligand (**2**) chelates the Pd(η^3-C_6H_9) moiety.[10] This was identified as an intermediate capable of leading to high asymmetric induction on attack of, for example, a malonate anion nucleophile, Scheme 1. Detailed NMR studies, facilitated by isotopic labelling, in conjunction with MM-DFT simulations, led to a model[10] in which the amide units in the catalyst facilitate enantioselective ligand-accelerated catalysis.[11]

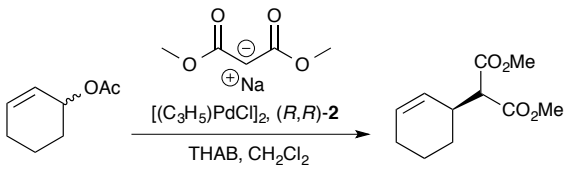

Scheme 1. Asymmetric allylic alkylation of racemic 2-cyclohexenyl acetate; **2** = 1,2-diaminocyclohexane TML ligand, THAB = tetrahexylammonium bromide.

For the ligand-accelerated catalysis to function efficiently, cation $[\mathbf{1}]^+$ requires a degree of flexibility. This flexibility is provided by the 13-membered chelate ring, but at a cost: complex $[\mathbf{1}]^+$ can readily undergo ring-opening oligomerisation to generate polynuclear species $([\mathbf{1}]^+)_n$, Scheme 2.[12] Competing nucleophilic attack of the oligomer, rather than the monomer

$[\mathbf{1}]^+$ is, in part, responsible for a reduction in overall enantioselectivity under non-optimised conditions.[13,14]

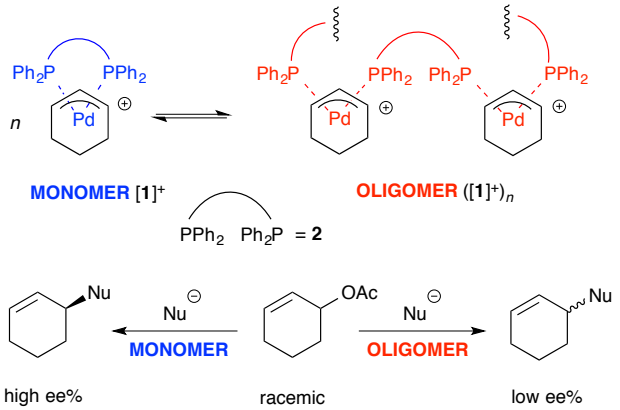

Scheme 2. Oligomerisation of $[\mathbf{1}]^+$ erodes enantioselectivity during asymmetric Pd-catalysed allylic alkylation mediated by **2** (as Scheme 1). Nu = nucleophile.

To date, the structure and driving forces for formation of the polynuclear oligomeric species has not been studied in detail. Herein we describe an investigation of the oligomerisation of D_0 and D_{47} isotopologues of $[\mathbf{1}]^+$, employing NMR spectroscopy, molecular mechanics (MM), molecular dynamics (MD), and small-angle neutron scattering (SANS). The data obtained indicate that the impact of a first-stage of depletion of the monomeric species $[\mathbf{1}]^+$ from the catalyst pool, via cyclic oligimerisation, is amplified by a second-stage process involving columnar aggregation of the oligomers, leading to species with very high nuclearity (up to 56 Pd centres). The effects of solvent, ligand enantiopurity and counter-ion on the degree of aggregation are explored in detail, and it is concluded that a relatively small and restricted set of conditions facilitate dissolution of the complexes in a low aggregation state, consistent with the extensive optimisation frequently required for these catalyst systems.

Results and Discussion

Preliminary NMR Studies and Synthesis of $[D_{47}]$-[1][$B(C_6F_5)_4$].

Despite extensive efforts,[15] we have been unable to crystallise any Pd(η^3-C_6H_9) complexes of **2**, in either oligomeric or monomeric forms. Indeed, to date, the only the X-ray crystal structures of Pd-allyl complexes of Trost ligand **2**[16] are η^3-C_3H_5 complexes with triflate counter anions: one a racemic tetranuclear cyclo-oligomer,[12] the other an acyclic dinuclear bis-P,O-chelate.[17]

The extent of solution-phase oligomerisation of cationic complexes of type $[\mathbf{1}]^+$ can be conveniently determined $^{31}P\{^1H\}$ NMR spectroscopy.[10,12] Analysis of [(*R*,*R*)-[**1**][BAr_4] complexes in CH_2Cl_2, where Ar = C_6Cl_5, 3,5-$(CF_3)_3C_6H_3$, or C_6F_5 ('BAr_F', Figure 1), indicates a maximum monomer concentration ($[\mathbf{1}]^+$) of about 4 mM. In THF the monomer maximum is lower (approx. 1.6 mM) and decreases as $[Pd]_{tot}$ is raised above 10 mM. With smaller, less charge-diffuse, counter-anions such as chloride or triflate, the monomer maxima are lower still. We were unable to fit simple analytical solutions[18] for monomer-oligomer distributions to any of the ^{31}P NMR data, indicative that physicochemical effects dominate over simple solution-phase equilibria, even at low $[Pd]_{tot}$.

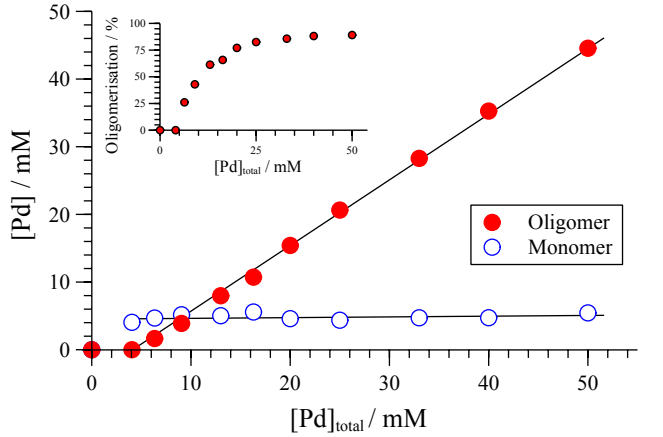

Figure 1. Speciation of [(*R*,*R*)-**1**][BAr_F] (BAr_F = $B(C_6F_5)_4$) determined by $^{31}P\{^1H\}$ NMR (CD_2Cl_2, 25 °C). Solid lines through data are solely a guide to the eye.

We thus elected to study the oligomeric species by SANS – a technique that can be used for characterising the shape and dimensions of large scale molecular aggregates and colloids in solution.[19] We began with [(*R*,*R*)-[**1**][BAr_F],[20] and, to aid the studies, also synthesised the perdeuterated enantiomeric complex [(*S*,*S*)-$[D_{47}]$-**1**][BAr_F]. Not only does this facilitate SANS in a non-deuterated solvent, thus providing greater neutron scattering contrast,[19] it also allows pseudo racemic and pseudo scalemic mixtures to be prepared by mixing [(*S*,*S*)-$[D_{47}]$-**1**][BAr_F] with [(*R*,*R*)-[**1**][BAr_F]. The perdeuterated complex was synthesised from benzoic acid ($[D_5]$-**3**), chlorobenzene ($[D_5]$-**4**) and cyclohexene ($[D_{10}]$-**5**), Scheme 3. A major hurdle was the *ortho*-metallation of ester $[D_5]$-**6** with $(TMP)_2Mg{\cdot}LiCl$,[21] which proceeded with an unexpectedly large net kinetic isotope effect ($k_H/k_D \approx 30$).[22] This required an excess base to be employed, and interfered with a planned direct phosphination of the metallated intermediate. Instead, the intermediate was trapped with I_2. The iodide $[D_4]$-**7** was then converted to a more conventional Grignard reagent,[23] before reaction with chlorophosphine $[D_{10}]$-**8**[10,24] to give phosphine $[D_{14}]$-**9**, and thus acid $[D_{14}]$-**10**.[25]

Cyclohexene $[D_{10}]$-**5**,[26] was epoxidised, to give $[D_{10}]$-**11**, and this ring-opened[27] to give aminoalcohol $[D_{10}]$-**12**.[28] Aziridine $[D_{10}]$-**13**, obtained via Mitsunobu conditions, was converted to azide $[D_{10}]$-**14**.[29] After diastereoisomer separation, hydrogenolysis,[30] gave (*S*,*S*)-diamine $[D_{10}]$-**15** which was coupled with acid $[D_{14}]$-**10** to afford Trost ligand $[D_{38}]$-**2**. The chloro-dimer $[D_9]$-**16**, prepared[31] from $[D_{10}]$-**5**, was converted to cationic complex $[D_9]$-**17,** and then reacted with $[D_{38}]$-**2** to generate [(*S*,*S*)-$[D_{47}]$-**1**][BAr_F] in good yield.

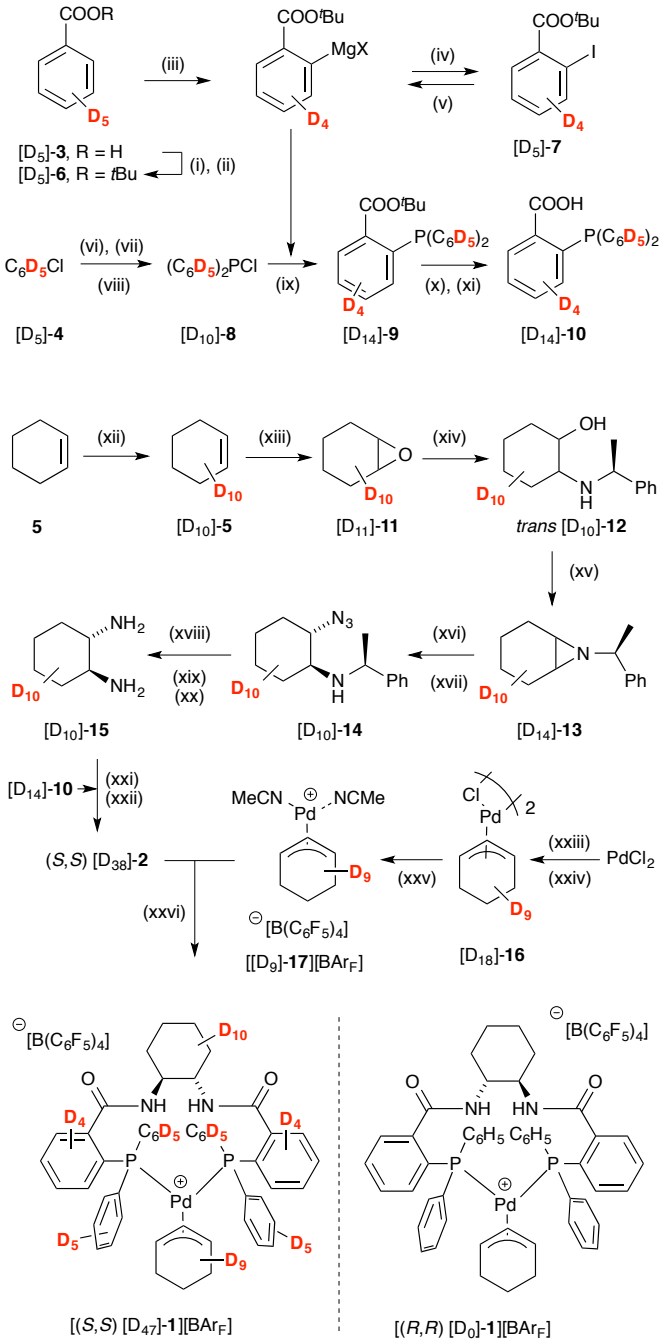

Scheme 3. Synthesis of pseudo enantiomer [(*S*,*S*)-[D$_{47}$]-**1**][BAr$_F$]; BAr$_F$ = B(C$_6$F$_6$)$_4$. Conditions: (i) $SOCl_2$, toluene, 100 °C; (ii) KO^{t}Bu, THF 0 °C; 84%; (iii) $(TMP)_2Mg \cdot 2LiCl$, THF, 0 °C to 30 °C; (iv) I_2, THF, -30 °C; 49%; (v) ^{i}PrMgCl, THF, - 40 °C, 2 h; (vi) Mg, LiCl, THF, reflux; (vii) Et_2NPCl_2, THF; (viii) HCl, Et_2O, -40 °C; 29%; (ix) [D$_{10}$]-**8** drop-wise addition, THF, -78 °C; 68%; (x) KOH, THF, r.t., 24 h; (xi) HCl; 58%; (xii) 5% $Ru(PPh_3)_3Cl_2$, D_2O, 10% SDS, microwave, 140 °C, 1 h; (xiii) *m*CPBA, CH_2Cl_2, $NaHCO_3$; 51%; (xiv) (*S*)-1-phenylethylamine, MeCN, LiBr, 60 °C; 74%; (xv) DIAD, PPh_3, THF, 0 °C to r.t.; 62%; (xvi) NaN_3, $CeCl_3 \cdot 7H_2O$, MeCN / H_2O 9:1, reflux; (xvii) silica-gel chromatography; 61%; (xviii) 20% $Pd(OH)_2$/C, MeOH, r.t., 1 atm H_2; (xix) 20% $Pd(OH)_2$/C, MeOH, 2M HCl / Et_2O, HCO_2NH_4, 65 °C; (xx) KOH, CH_2Cl_2, r.t.; (xxi) EDCI·HCl, HOBt·H_2O, iPr_2NEt, CH_2Cl_2, r.t.; (xxii) Et_2O, HCl; 30%; (xxiii) NaCl, NaOAc, $CuCl_2$, AcOH, Ac_2O, 2 h, 95 °C; (xxiv) [D$_{10}$]-**5**, 60 °C, 20 h; 13% (xxv) KBAr$_F$, MeCN, CH_2Cl_2, r.t.; (xxvi) CH_2Cl_2, r.t.; 99%. See supporting information for full details.

SANS Analysis of Aggregation of [1][BAr$_F$] in THF

We began SANS analysis[32] of enantiopure [(*R*,*R*)-**1**][BAr$_F$] in THF-D$_8$ at 25 °C, with [Pd]$_{tot}$ concentrations at and above the oligomerisation threshold (1.6 to 64 mM). The combined data sets,[33] presented here as plots of scattered intensity ($I(Q)$, *y*-axis) versus neutron momentum transfer (Q, *x*-axis) were analysed with standard mathematic models corresponding to various simple shapes,[19] Figure 2.[34] This clearly identified the particles as cylindrical or rod-like, and Guinier analyses (see supporting information, Figure S69) established the radii (8-9 Å) and length (150-200 Å) as invariant across the range of [Pd]$_{tot}$ explored. In other words, the number of particles changes in response to [Pd]$_{tot}$, but not their average dimensions,[35] clearly indicative of a set of factors that tightly control the particle scale.

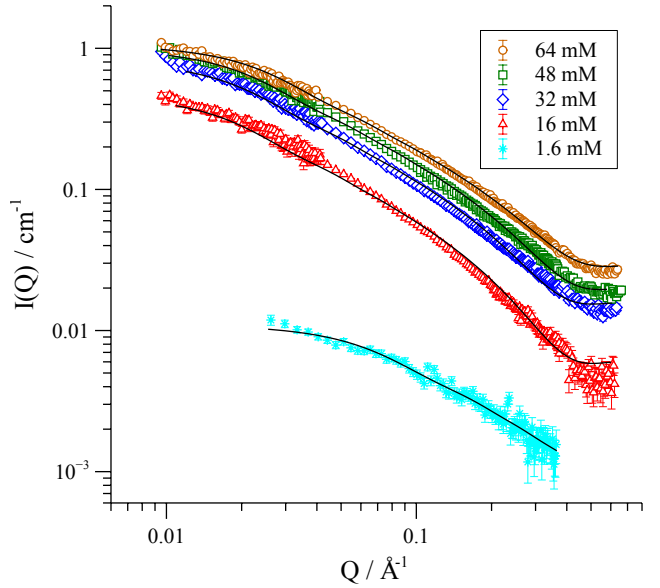

Figure 2. SANS profiles of 0.25-10.0 wt/vol% {[(*R*,*R*)-**1**][BArF]}$_n$ in THF-D$_8$, 25 °C; I(Q) = scattered intensity, Q = neutron momentum transfer = 2πθ/λ; where detector angle = θ and neutron wavelength = λ. The curves that are fitted correspond to that expected for a cylindrical particle.

We have previously used ^{31}P NMR to analyse the constitution of the solution-phase (i.e. lower-order) oligomers generated from various complexes of type [**1**][BAr$_4$] in CD_2Cl_2.[10,12] Using PPCOSY in combination with pairs of isotopically-differentiated ligands ([D$_n$]-**2**), we were able to determine that the oligomers are: i) non-chelated species, i.e. each of the ligands (**2**) in the oligomer are coordinated to two different Pd centres; ii) present in predominantly homochiral form, i.e. [(*R*,*R*)-**1**]$^+$ and [(*S*,*S*-**1**]$^+$ oligomerise independently, and iii) there no free (i.e. not Pd-coordinated) P-centres in the ligand (**2**). Although a cyclic oligomer structure (Scheme 2) is fully consistent with these features, we were unable to determine the number (n) of ring-opened monomer units incorporated within the cyclo-oligomer ([**1**][BAr$_4$])$_n$.

As [Pd]$_{tot}$ in THF or CH_2Cl_2 solutions of complexes of type [**1**][BAr$_4$] is increased, the ^{31}P NMR bandshape of the signals

arising from the cyclo-oligomer do not change in appearance, but the samples do become increasingly turbid. This behaviour suggests that in response to an increase in $[Pd]_{tot}$, cyclo-oligomers $([\mathbf{1}][BAr_4])_n$ do not incorporate more monomer (n), but instead aggregate to form large particles, $\{([\mathbf{1}][BAr_4])_n\}_m$, containing '$m$' cyclo-oligomers. It is these high nuclearity particles that are detected by SANS.[12]

In racemic or scalemic samples of ($[\mathbf{1}][BAr_F]$), the homochiral cyclo-oligomers, $([\mathbf{1}][BAr_F])_n$, could aggregate in three general forms: discrete homochiral, ordered heterochiral (e.g. alternating or co-block), or statistically distributed. SANS data of mixtures of $[(R,R)\text{-}\mathbf{1}][BAr_F]$ and $[(S,S)\text{-}\mathbf{1}][BAr_F]$ representing enantiopure, scalemic, and racemic samples, was uniform across the series, within experimental error, Figure 3.

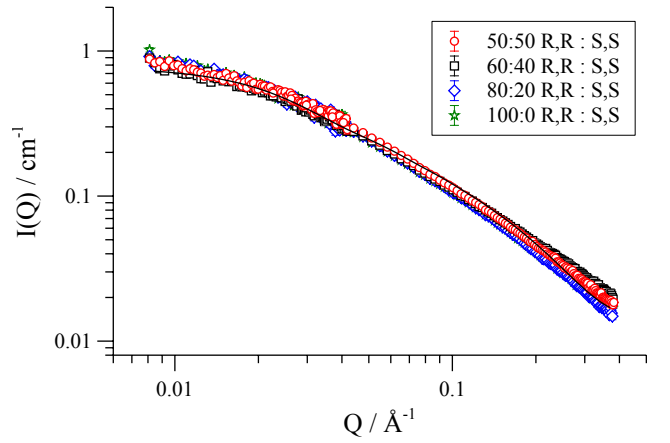

Figure 3. Fitted SANS profiles of 32 mM enantio-pure, racemic and scalemic samples of $[\mathbf{1}][BAr_F]$ in THF-D_8, 25 °C.

The absence of a change in particle number,[36] shape or size, suggests a statistical distribution.

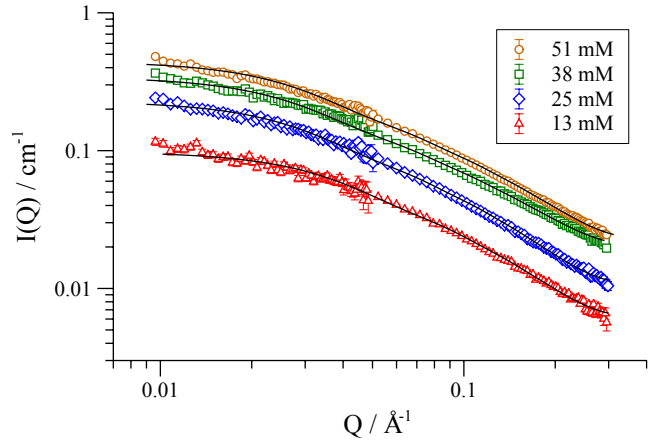

Figure 4. SANS data for pseudo racemic complex $[(S,S)\text{-}[D_{47}]\text{-}\mathbf{1}][BAr_F]$ + $[(R,R)\text{-}[D_0]\text{-}\mathbf{1}][BAr_F]$) in THF-$D_8$ at 25 °C, at $[Pd]_{tot}$ ranging from 13 to 51 mM.

SANS data of the pseudoracemate ($(S,S)\text{-}[D_{47}]\text{-}\mathbf{1}][BAr_F]$ + $[(R,R)\text{-}[D_0]\text{-}\mathbf{1}][BAr_F]$) in D_0-THF, and in D_8-THF, Figure 4, and enantiomerically pure $[(S,S)\text{-}[D_{47}]\text{-}\mathbf{1}][BAr_F]$ in D_0-THF, show that the fully and partially deuterated systems retain the concentration-independent, cylindrical shape in the aggregate. The main difference however is in the dimensions: $[D_{47}]\text{-}[\mathbf{1}][BAr_F]$ forms shorter (130 Å), slightly wider (10 Å radius) cylinders than $[D_0]\text{-}[\mathbf{1}][BAr_F]$. The pseudo racemic mixture measures as an average of its precursors (9-10 Å radius, 150 Å length), again consistent with a statistical distribution of cyclo-oligomers in the aggregate.[37]

Molecular Mechanics (MM) and Dynamics (MD)

Computational modelling was employed to probe the factors that control the aggregation phenomena, and to estimate the size (n) and number of cyclo-oligomers in the particle (m). The number of atoms in the aggregates (>6,000, *vide infra*) means that density functional theory (DFT) calculations of their structures would demand currently unattainable computational resources and inordinate simulation times. On the other hand, molecular mechanics (MM) can provide a good approximation, in just a small fraction of the computational time required by DFT. We began by confirming that structure of the 84-atom monomeric cationic P,P-chelate $[\mathbf{1}]^+$, optimised at MM3[38] theory level and dielectric constant $\varepsilon = 9.0$, was almost identical to that obtained using DFT[39] (B3LYP-D3) in a polarisable continuum model for dichloromethane. Further calculations involving ion-pairs, oligomers and aggregates were then performed using MM3,[40] to provide analysis of the energies involved, albeit at a course-grained level of detail.

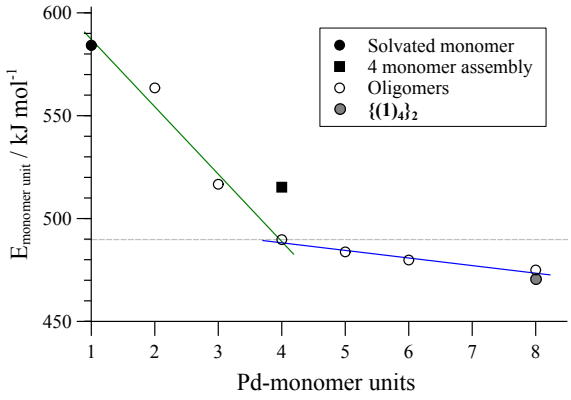

Figure 5. MM3 energies of cyclo-oligomeric complexes $([\mathbf{1}][BAr_F])_n$; $\varepsilon = 9.0$

Comparison of the MM3 optimised energies for monomeric P,P-chelate [1][BArF] with a series of homochiral cyclo-oligomers, $([\mathbf{1}][BArF])_n$, normalised by the number of Pd atoms (n, the x-axis in Figure 5) confirmed cyclo-oligomerisation to be exergonic. The cyclic dimer ($n = 2$) still suffers from ring strain, and a more substantial stability is afforded by trimerisation ($n = 3$) then tetramerisation[41] ($n = 4$, Figure 6). Further increase in oligomer ring size ($n = 5, 6, 8$) yields a modest reduction in the system energy and generates species with significantly higher radii than the 8-9 Å cylinder radius detected by SANS.

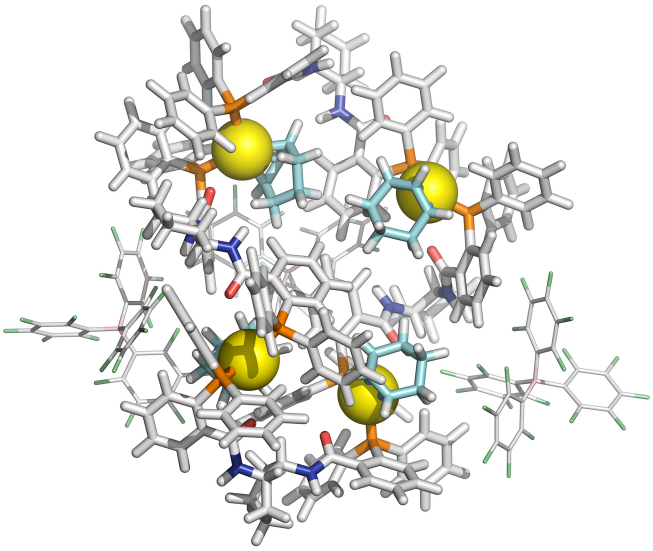

Figure 6. MM3 structure of tetranuclear cyclo-oligomer $([\mathbf{1}][BAr_F])_4$. For clarity, only two of the four BAr_F anions are shown. Colour coding: Pd, yellow; P, orange; O, red; N, dark blue; C, light grey; B, pink; F, green; η^3-C_6H_9, light blue.

Aggregation of cyclic tetramers $([\mathbf{1}][BAr_F])_4$ was then probed by MM3 as a mechanism for generation of cylindrical particles. Positively charged rod-like structures with dissociated or removed anions were estimated by MM3 to be very much higher in energy.

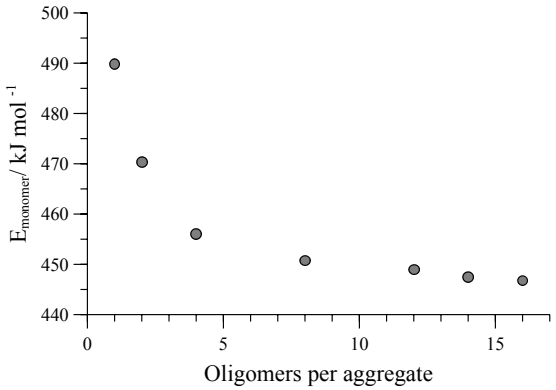

Figure 7. MM3 energies normalised per monomer of aggregates $\{([\mathbf{1}][BAr_F])_4\}_m$ at ε = 9.0; *x*-axis is the number of tetramers (*m*) in the aggregate.

Although BAr_F is considered a weakly coordinating anion,[42] the charge delocalisation over its surface reduces repulsive interactions with other BAr_F anions as well as making it significantly lipophilic. Indeed, the calculations indicated a favourable interleaving of the anions in sandwich layers[43] between cationic cyclo-oligomers. The estimated formation energies, (ΔE, Figure 7) of such species $\{([\mathbf{1}][BAr_F])_4\}_m$ as a function of '*m*' indicated that columnar aggregates are readily attainable, with the growing entropic cost ($T\Delta S$) placing limits on the aggregate length.

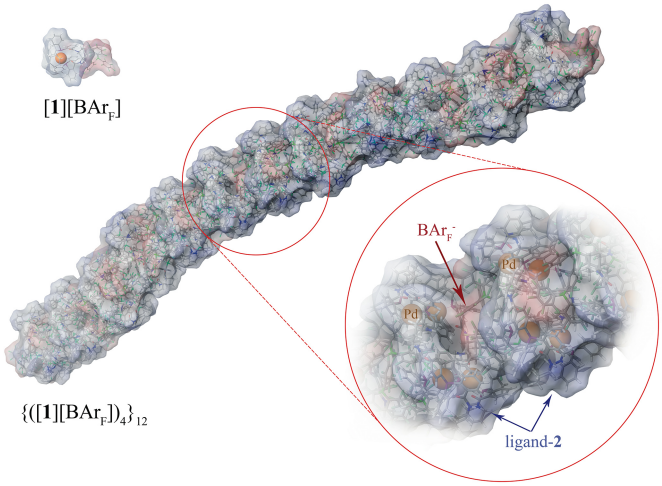

Figure 8. MM3 structure of $\{([\mathbf{1}][BAr_F])_4\}_{12}$. The monomer $[\mathbf{1}][BAr_F]$ (top left), with palladium coloured orange, is shown for scale.

These conclusions were further probed by molecular-dynamics (MD) simulations in which the MM3-minimised structures $\{([\mathbf{1}][BAr_F])_4\}_m$ were computationally excited over a short period (300 ps) to test the structural integrity of the aggregate as a function of '*m*'. In the low dielectric constant medium used for the model, most systems (*m* = 4 to 16) did not undergo any significant changes in their tertiary structure at 300 K, over the full 300 ps simulation time. As the energy input was increased the aggregate models exhibited varying degrees of structural deformation and at 600-700 K rapidly fragmented. The most significant observations were made in the intermediate region (500-550 K) where aggregates with *m* = 10-14 (e.g. Figure 8, *m* = 12) retained a cylinder shape, albeit mildly distorted, whereas higher or lower order aggregates significantly deformed, in some cases losing one or more BAr_F anions. The average dimensions of the MM3 aggregates with *m* = 10-14 (radius 8-9 Å and length 150-200 Å) are fully consistent with the dimensions determined by SANS.

The Effect of Counter-ion and Solvent on Shape and Extent of Aggregation

The effect of solvent on aggregation was probed by MM, $^{31}P\{^1H\}$ NMR (Figure 9) and SANS, also comparing $[\mathbf{1}][BAr_F]$ with $[\mathbf{1}][OTf]$ to explore the impact of counter-ion. The aggregation mode for $[\mathbf{1}][BAr_F]$ determined by MM3, e.g. Figure 8, involves multiple close-range electrostatic interactions that reduce the overall system energy. It is thus not surprising that the solvent dielectric constant, ε_r, was found to modulate aggregation,[44] and thus also solubility: precipitation being the consequence of complete aggregation. As indicated in Figure 9, both $[\mathbf{1}][OTf]$ and $[\mathbf{1}][BAr_F]$ readily oligomerise and in all of the solvents that were explored, becoming essentially insoluble at the extremes of ε_r, e.g. in alkanes, most ethers, chloroform, aromatic hydrocarbons, and at the opposite end of the scale, in water. The lipophilicity and charge density of the anion also affects the solubility: $[\mathbf{1}][BAr_F]$ readily dissolves in

THF, while [**1**][OTf] does not, and at the opposite end of the ε_r scale, [**1**][OTf] is soluble in aqueous-organic mixtures, whereas [**1**][BAr_F] is not.

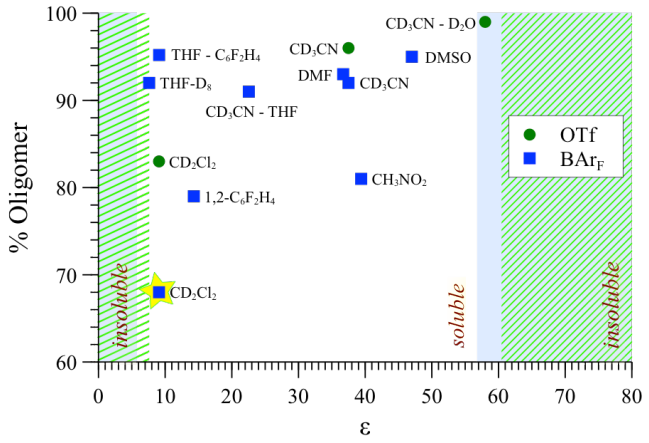

Figure 9. Oligomerisation of [**1**][BAr_F] and [**1**][OTf] at $[Pd]_{tot}$ = 15 mM in various solvents, as determined by ^{31}P NMR; overlaid areas in green (OTf) and blue (BAr_F) indicate regions in which the complexes are insoluble.

SANS was employed to explore how the macromolecular composition of aggregates $\{([\mathbf{1}][X])_n\}_m$ is affected by solvation. Although [**1**][BAr_F] is not soluble in organic-aqueous mixtures, SANS data was attainable in polar aprotic solvents (e.g. MeCN, ε_r = 37.5; and DMSO, ε_r = 47). This confirmed that cylindrical aggregates were still formed, but were significantly shorter than those in THF, Figure 10. Medium length cylinders were detected in a 50:50 mixture of THF and acetonitrile, consistent with the intermediate solvent polarity ($\varepsilon_r \approx 23$). In all cases, the cylinders were of radius 8-10 Å, strongly suggesting the prevalence of the tetranuclear cyclo-oligomer building blocks, with the solvent modulating the aggregation number '*m*': $\{([\mathbf{1}][BAr_F])_4\}_m$.

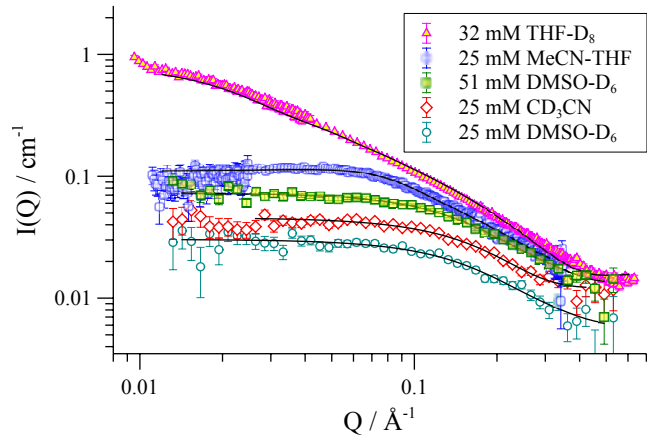

Figure 10. SANS data for [**1**][BAr_F] in various solvents at 25 °C.

The [**1**][OTf] aggregates behaved differently. Although, cylinders of radius 8-10 Å were again detected in all cases, indicative of $\{([\mathbf{1}][OTf])_4\}_m$ aggregates, the flexibility, lengths and charge distribution in the particles were very different to those formed from [**1**][BAr_F]. In CD_2Cl_2, [**1**][OTf] forms long cylinders (up to 160 Å; Figure 11) that are semi-flexible, a phenomenon that can be attributed to the small and interactive triflate anion being less able to rigidify the structures than the larger and more lipophilic BAr_F anion.

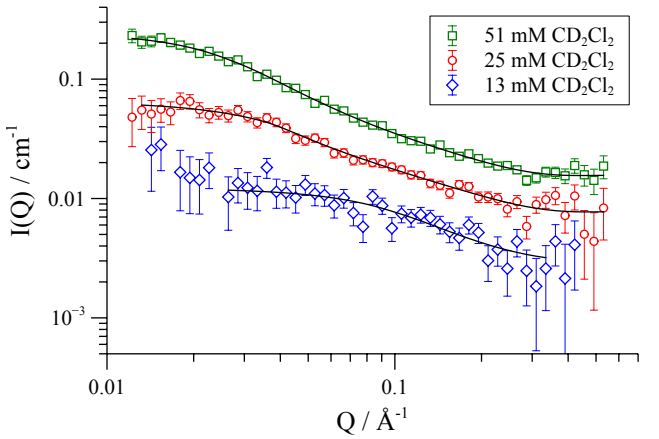

Figure 11. SANS for [**1**][OTf] in CD_2Cl_2 at 25 °C.

The anion effect became even more pronounced in media of higher dielectric constant. The SANS data indicated the presence of charged particles in acetonitrile-based solvent mixtures (ε_r = 47-58), Figure 12, indicating solvation-induced ion-pair separation of the triflate from the cationic Pd(II) oligomeric core. The increased cationic repulsion between the cyclo-oligomers thus results in much shorter cylinders, just 30 Å in length, with misleadingly simple ^{31}P NMR spectra.[45] Similar conclusions were drawn from MD simulations with the medium set at ε_r = 35: only the shortest aggregates $\{([\mathbf{1}][OTf])_4\}_{2\text{-}4}$ were structurally stable at elevated energies (500 K; 300 ps).

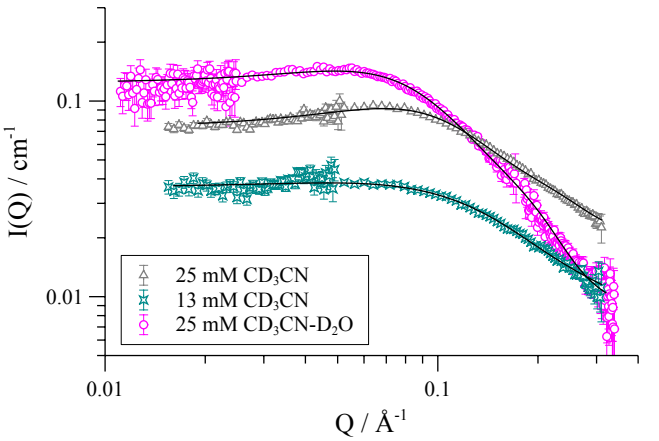

Figure 12. SANS for [**1**][OTf] in CD_3CN at 25 °C.

Finally, to probe the relevance of the higher aggregates to asymmetric alkylation (Scheme 1) SANS data was acquired on reaction mixtures in which [**1**][BAR_F] was employed as a pre-

catalyst (10 mol%) for addition of tetrabutylamonium dimethylmalonate to cyclohexenylacetate in THF. While the effects of substrate background scattering, varying acquisition times and shorter Q-range slightly affected the accuracy of data, it remained clear that the dominant structures in solution were large cylinders, for the whole duration of the catalytic process. This result is consistent with previous conclusions that in THF the catalytic turnover proceeds via a small pool of highly-active monomeric catalyst species, in competition with cyclo-oligomers and aggregates.[10,12]

Conclusions

Since the initial report that $[\mathbf{1}]^+$ readily oligomerises,[13] and that this is a largely undesirable property of an otherwise highly efficient catalyst, e.g. Scheme 1, there has been limited understanding of the oligomer structure.[10,12] We have now identified, through NMR, SANS, and MM/MD simulations of $[D_n]$-$[\mathbf{1}][BAr_F]$ (n = 0, 47),[46] that monomeric cations $[\mathbf{1}]^+$ undergo chelate-opening to form a tetranuclear cyclo-oligomer; this being thermodynamically favoured over higher and lower nuclearity species. A second-stage process involving columnar type interactions between the cyclo-oligomers then forms polynuclear aggregates. For $[\mathbf{1}][BAr_F]$ in THF, these comprise 10-14 alternating layers of cyclo-oligomer and interleaved BAr_F anions, containing up to 56 Pd(η^3-C_6H_9) centres, ligands (**2**) and anions, and generate cylindrical particles of radius 8-9 Å and length 150-200 Å.

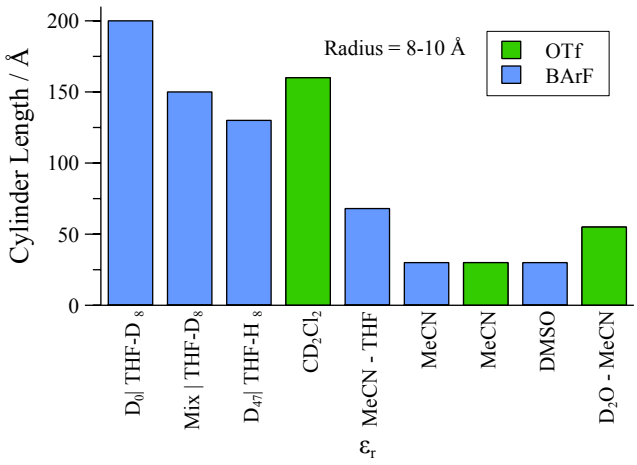

Figure 13. Summary of upper-range aggregate cylinder lengths of [**1**][BArF] and [**1**][OTf] samples, as determined by SANS experiments, in selected solvents.

The identity of the counter-anion has a pronounced effect on the proportion of oligomer generated from the monomer. Bulky, weakly-coordinating anions,[47] reduce the extent of oligomerisation, particularly in low polarity solvents that cannot effectively stabilise charged particles. Here the role of the bulky and relatively lipophilic anions is to solvate the monomer $[\mathbf{1}]^+$. Smaller harder, less lipophilic anions are less able to solvate the monomer, and have the indirect effect of shifting the equilibrium towards the oligomer; an undesirable feature for catalysis. The diminutive size of the anion also results in greater flexibility of the resulting columnar aggregates, which are more ionic in nature, reducing their solubility in less polar solvents.

Overall, although the solvent polarity, counter-anion (X), and net concentration ($[Pd]_{tot}$) all contribute to determining the degree of oligomerisation and aggregation (Figure 13) of monomer [**1**][X], the solvent perhaps offers the greatest degree of scope for optimisation under the conditions of catalysis. In this regard, CH_2Cl_2 is favourable: solutions can be virtually free of oligomer at ambient temperature, provided $[Pd]_{tot} \leq 4$ mM. Intriguingly, SANS studies of non-ionic surfactants[48] have revealed specific solvent combinations that can lead to "dead zones" where aggregation is supressed, even for concentrated monomer solutions. If such "dead zone" solvent combinations can be found for complexes of type [**1**][X], this may be highly advantageous for improving catalytic productivity whilst maintaining selectivity.

Acknowledgements

We thank the ILL (France), ISIS (UK), and STFC (UK) for facilities, and Dr S Rogers and Dr I Grillo, for expert technical assistance. The Bristol Chemical Synthesis Centre for Doctoral Training (EPSRC EP/G036764/1), AstraZeneca and the University of Bristol provided a PhD studentship to DTR. GCLJ was a Wolfson Research Merit Award Holder whilst this research was conducted.

Notes and references

[a] *School of Chemistry, University of Glasgow, Joseph Black Building, University Ave, Glasgow, Lanarkshire G12 8QQ, UK. Tel: +44 (0) ; E-mail: daugirdas.racys@glasgow.ac.uk*
[b] *School of Chemistry, University of Bristol, Office S314, Cantock's Close, Clifton, Bristol BS8 1TS, UK. Tel: +44 (0) 117 928 9180; E-mail: Julian.Eastoe@bristol.ac.uk*
[c] *School of Chemistry, University of Edinburgh, Joseph Black Building, West Mains Road, Edinburgh, Scotland EH9 3JJ, UK. Tel: +44 (0) 131 650 4795; E-mail: guy.lloyd-jones@ed.ac.uk*
[d] *University of Gothenburg, Department of Chemistry and Molecular Biology Kemigården 4, #8076, SE-412 96 Göteborg, Sweden; E-mail: pon@chem.gu.se*

Electronic Supplementary Information (ESI) available: Synthesis and Characterisation of compounds, and full details of aggregation studies by NMR, SANS, and MM3. See DOI: 10.1039/b000000x/

1. B. M. Trost, M. R. Machacek, A. Aponick, *Acc. Chem. Res.* 2006, **39**, 747-760.
2. Z. Lu, S. Ma, *Angew Chem. Int. Ed.* 2007, **47**, 258-297.
3. Trost, B. M.; Bunt, R. C. *J. Am. Chem. Soc.*, **1994**, *116*, 4089-4090.
4. Fuchs, S.; Berl, V.; Lepoittevin, J.-P. *Eur. J. Org. Chem.* **2007**, *7*, 1145-1152.
5. Trost, B. M.; Toste, F. D. *J. Am. Chem. Soc.*, **2003**, *125*, 3090–3100.
6. Trost, B. M.; Dong. G. *J. Am. Chem. Soc.* **2006**, *128*, 6054-6055.
7. Trost, B. M.; Asakawa, N. *Synthesis* **1999**, 1491–1494.
8. B. M. Trost, R. C. Bunt, *J. Am. Chem. Soc.*, 1996, **118**, 235.
9. G. C. Lloyd-Jones, S. C. Stephen, *Chem. Eur. J.*, 1998, **4**, 2539-2549.

10. C. P. Butts, E. Filali, G. C. Lloyd-Jones, P.-O. Norrby, D. A. Sale, Y. Schramm, *J. Am. Chem. Soc*. 2009, **131**, 9945-9957.
11. D. J. Berrisford, C. Bolm, K. B. Sharpless, *Angew. Chem., Int. Ed.* 1995, **34**, 1059-1070.
12. J. Eastoe, I. J. S. Fairlamb, J. M. Fernández-Hernández, E. Filali, J. C. Jeffery, G. C. Lloyd-Jones, A. Martorell, A. Meadowcroft, P.-O. Norrby, T. Riis-Johannessen, D. A. Sale; P. M. Tomlin, *Faraday Discuss*. 2010, **145**, 27-47.
13. I. J. S. Fairlamb, G. C. Lloyd-Jones, *Chem. Commun*, 2000, 2447-2448.
14. Stoichiometric reaction of [(*R*,*R*)-[**1**][BAr_4] (Ar = 3,5-$(CF_3)_3C_6H_3$) with tetrabutylammonium dimethylmalonate in THF at 21 °C: $[Pd]_{tot}$ = 1 mM affords alkylation product in 98% ee, whereas product of 6 % ee is obtained when $[Pd]_{tot}$ = 27 mM.[10]
15. Around 100 attempts were made to crystallise the following complexes ([(*R*,*R*)- and rac [**1**][X], X = BAr_F,, B(3,5-$(CF_3)_3C_6H_3)_4$, [$Al(OC(CF_3)_3)_4$] and OTf) using diffusion, evaporation, cooling, seeding, co-crystallisation, and other methods, from a variety of binary and ternary solvent mixtures, including but not limited to chloroform, CH_2Cl_2 / pentane, 1,2-dichloroethane / hexane, THF / heptane, 1,2-difluorobenzene / 1,3-difluorobenzene, tetrachloroethane / hexafluorobenzene, MeCN / mesitylene, aqueous MeCN / MTBE, water, diethyl ether, etc. without success.
16. For examples of X-ray structures of Pd complexes of **2** that are inactive as catalysts for allylic alkyation, see: a) K. R. Campos, M. Journet, S. Lee, E. J. J. Grabowski, R. D. Tillyer, *J. Org. Chem.* 2005, **70**, 268-274; b) C. Amatore, A. Jutand, L. Mensah, L. Ricard, *J. Organomet. Chem*. 2007, **692**, 1457–1464.
17. C. P. Butts, J. Crosby, G. C. Lloyd-Jones, S. C. Stephen, *Chem. Commun*. 2000, 1707-1708.
18. D. C. Smith and G. M. Gray, J. Chem. Soc., Dalton Trans., 2000, 677.
19. J. Eastoe, *Surfactant Chemistry*, Wuhan University Press, Wuhan, China, 2005.
20. Perfluoro tetraphenylborate $[B(C_6F_5)_4]^-$ ("BAr_F") was chosen to avoid SANS data being complicated by neutron scattering from protons or deuterons in the counter-ion, as this could then be used without perturbation in the perdeuterated complex.
21. C. J. Rohbogner, A. J. Wagner, G. C. Clososki, P. Knochel, *Org. Synth.* 2009, **86**, 374-384.
22. The large KIE, estimated as $k_H/k_D \approx 30$, by comparison of approximate rates of metallation of the non-deuterated substrate, may arise from multiple primary effects, involving the TMP-amide, and in situ generated [D]-TMP, or from tunnelling.
23. To avoid the formation of by-products, it was found that it was essential to slowly add D_{10}-chlorodiphenylphosphine [D_{10}]-**8** to the Grignard drop-wise at -78 °C.
24. F. M. Piller, P. Appukkuttan, A. Gavryushin, M. Helm, P. Knochel, *Angew. Chem. Int. Ed*. 2008, **47**, 6802-6806.
25. E. Filali, G. C. Lloyd-Jones, D. A. Sale, *Synlett*, 2009, 205-208.
26. K. Ishibashi, S. Matsubara, *Chem. Lett*. 2007, **36**, 724-725.
27. M. Chandrasekhar, G. Sekar, V. K. Singh, *Tetrahedron Lett*. 2000, **41**, 10079-10083.
28. A. K. Chakraborti, S. Rudrawar, A. Kondaskar, *Eur. J. Org. Chem*. 2004, 3597-3600.
29. V. M. Mastranzo, E. Santacruz, G. Huelgas, E. Paz, M. V. Sosa-Rivadeneyra, S. Bernès, E. Juaristi, L. Quintero, C. A. de Parrodi, *Tetrahedron: Asymmetry* 2006, **17**, 1663-1670.
30. In contrast to the report of Singh,[27] hydrogenolysis with $Pd(OH)_2$/C under acidic conditions in methanol failed to cleave the α-methylbenzyl auxiliary. Instead, after reduction of the azide, the hydrogen source was changed to ammonium formate: a) WO 2005/092840 PCT/IB2005/000619; b) T. Bieg, W. Szeja, *Synthesis* 1985, 76-77.
31. The dimer was prepared using the literature procedure (see: a) B. M. Trost, P. E. Strege, L. Weber, T. J. Fullerton, T. J. Dietsche, J. Am. Chem. Soc. 1978, **100**, 3407–3415; b) S. Imaizumi, T. Matsuhisa, Y. Senda, *J. Organomet. Chem*. 1985, **280**, 441-448). However we identified degradation of the crude organometallic complex during the early work-up stages. Constant exposure of the crude material to air, avoiding vacuum operations until the complex has been purified, significantly increases the yield of **17**.
32. SANS experiments were conducted at the Institut Laue-Langevin (ILL) in Grenoble, France. Data was acquired in two detector movements on separate instrument: high-*Q* data on D16, and low-*Q* data on D22.
33. Very similar results were obtained on SANS2D at ISIS, UK using a different batch of complex, indicative of the reproducibility of the data.
34. Measurements were also conducted at higher and lower temperatures. Consistent with analysis by $^{31}P\{^1H\}$ NMR spectroscopy, aggregation is reversible, and favoured by lower temperatures.
35. At higher concentrations the radius shrank slightly, possibly due to the associated increase in the ionic strength of the medium.
36. It should be noted that most of the concentrations employed for the SANS experiments were, by necessity, well above the oligomerisation and aggregation threshold. Changes in particle number due to differential selectivity between homochiral and heterochiral aggregation of cyclo-oligomers may be small, and thus hard to distinguish.
37. The resolution of the SANS instrument was insufficient to completely rule out the possibility that the scattering profile is the composite of two curves arising from segregated (homochiral) cylinders.
38. Schrödinger MacroModel, version 9.9: Schrödinger, LLC, New York, NY, 2012.
39. Jaguar, version 7.9. Software: Schrödinger, LLC, New York, NY, 2012.
40. Schrödinger MacroModel, version 9.9: Schrödinger, LLC, New York, NY, 2012.
41. Comparison of the MM3 energy of the tetramer with a pre-orientated assembly of four P,P-chelates {4([**1**][BAr_F])}, or the energy of two non-covalently associated tetramers {([**1**][BAr_F])$_4$}$_2$ with a single cyclic octamer (Figure 5) again indicates that oligomerisation to form the tetramer (Figure 6) is most favourable. The dimensions of the MM3-minimsed tetramer, are similar to that of the Pd/ligand core of a cyclic tetranuclear complex [(η^3-C_3H_5-Pd)$_4$(**2**)$_4$][OTf_4], determined by single crystal X-ray diffraction.[12]
42. I. Krossing, I. Raabe, *Angew. Chem. Int. Ed*. **2004**, 43, 2066–90.

43. A variety of other anion arrangements explored by MM3 modelling did not reveal any plausible alternative modes of aggregation, that would be compatible with the SANS data.
44. The impact of solvent dielectric constant on ion-pair separation can be predicted by the Bjerrum length equation: $\lambda_B=e^2/(4\pi\varepsilon_0\ \varepsilon_r\ k_BT)$ which indicates that the ion separation distance, λ_B, is inversely proportional to the dielectric constant of the media in which the solute is dissolved. The equation presumes point charges, however the general principles may still apply to more complex systems such as [**1**][X].
45. These systems present an apparently simple pair of doublets (J = 38 Hz), almost identical in appearance, but not chemical shift, to the pair of doublets ($^{2Pd}J_{PP}$) in the monomeric chelate system. However, it is very evident from the SANS data that the solutions are dominated by oligomers $\{([\mathbf{1}][OTf])_4\}_m$, and from careful inspection of the ^{31}P NMR spectrum that the monomer is indeed also present, but only in very low proportions ($\leq$ 4%).
46. The enantiomerically pure species $[D_{47}]$-[**1**][BArF is among the most synthetically complex perdeuterated species to have been prepared to date. For other examples see: a) F. Aussenac, M. Laguerre, J.-M. Schmitter, E. J. Dufourc *Langmuir* **2003**, *19*, 10468-10479; b) R. G. Alken, US patent, US2005069276A1; c) M. Schulz, J. Hirschmann, A. Draksharapu, G. Bindra, S. Soman, A. Paul, R. Groarke, M. T. Pryce, M. S. Rau, W. R. Browne, J. G. Vos, *Dalton Trans.* **2011**, *40*, 10545-10552; d) T. Abe, A. Miyazawa, H. Konno, Y. Kawanishi, *Chem. Phys. Lett.* **2010**, *491*, 199-202; e) C. Lenges, P. White, M. Brookhart, *J. Am. Chem. Soc.* **1999**, *121*, 4385-4396; f) M. Ogasawara, K. Takizawa, T. Hayashi, *Organometallics* **2002**, *21*, 4853-4861; g) R. Brainard, T. Miller, G. Whitesides, *Organometallics* **1986**, *5*, 1481-1490.
47. All of the BAr_4 anions tested, as well as $Al(OR_F)_4$ ("Krossing anions": Krossing, I. *Chem. Eur. J.* **2001**, *7*, 490-502), were effective in this regard.
48. Hollamby, M. J.; Tabor, R.; Mutch, K. J.; Trickett, K.; Eastoe, J.; Heenan, R. K.; Grillo, I. *Langmuir* **2008,** *24,* 12235-12240.